Int. J. Microgravity Sci. Appl., **33** (1) (2016) 330104
DOI: 10.15011/ijmsa.33.330104

IIIII Development of Boiling and Two-phase Flow Experiments on Board ISS IIIII
(Original Paper)

Development of Boiling and Two-Phase Flow Experiments on Board ISS (Void Fraction Characteristics in the Observation Section just at the Downstream of the Heating Section)

Taisaku GOMYO [1], Hitoshi ASANO [1], Haruhiko OHTA[2], Yasuhisa SHINMOTO[2], Osamu KAWANAMI[3], Koich SUZUKI[4], Ryoji IMAI[5], Toshiharu OKA[6], Toshiyuki TOMOBE[6], Koushiro USUKU[6], Masaki SHIMADA[6], Masahiro TAKAYANAGI[7], Satoshi MATSUMOTO[7], Takashi KURIMOTO[7], Hidemitsu TAKAOKA[7], Michito SAKAMOTO[7], Atsushi OKAMOTO[7], Kenichiro SAWADA[7], Haruo KAWASAKI[7], Kiyosumi FUJII[8] and Kazumi KOGURE[9]

Abstract

An observation section has been developed for the detail observation of gas-liquid interfacial structure in boiling and two-phase flow experiments onboard International Space Station. A stereoscopic photography method was applied for 3D measurement using one high frame-rate camera, and the accuracy in measurement of liquid film thickness was evaluated. It was confirmed in the preliminary experiment that liquid film thickness could be measured from images within ± 5 % accuracy. Moreover, to evaluate the development of the flow structure from the exit of the heating section, flow observation and cross-sectional average void fraction measurement was performed at four locations at the downstream of the heating section. As the result, under the scondition where slug flow was observed in the developed region, the fluctuation band of void fraction was small just at downstream of the exit of the heating section due to many small bubbles in liquid slugs. Under the conditions where annular flow was observed in the developed region, annular flow had been already formed at the exit, and then liquid film thickness became thicker.

Keyword(s): One-component gas-liquid two-phase flow, ISS experiment, Flow pattern, Void fraction
Received 3 December 2015, Accepted 23 January 2016, Published 31 January 2016

1. Introduction

Two-phase flow loop thermal control system has been attracting attention as a cooling and heat management system for space structures to satisfy the requirements for heat rejection with higher heat flux and lager heat amount. The understanding of gas-liquid two-phase flow dynamics under microgravity is necessary for the design of the system. Especially, vapor liquid interfacial structure should be clarified to avoid a boiling crisis, such as dry-out and departure from nucleate boiling. Previously, numerous papers on gas-liquid two-phase flow characteristics under microgravity had been published, and were reviewed by Nancy and Colin[1)]. However, those were mainly for adiabatic air-water two-phase flows, because the microgravity period was limited depending on the experimental method, such as drop tower and parabolic flight of an airplane. Although some papers [2-6)] are on boiling two-phase flows, the difference in two-phase flow behaviors between normal and microgravity had not been exactly clarified. Therefore, flow boiling experiments are required to be performed under stable microgravity condition.

Under microgravity, the local slip velocity will be close to zero due to the dissipation of buoyancy force. Therefore, in a bubble movement in a pipe flow, the lateral force on bubbles will be close to zero, and bubbles will tend to flow in the straight line along the tube axis. Little slip velocity will lower the frequency of bubble coalescence. Such flow behavior will affect on the boiling flow characteristics at low vapor quality. On the other hand, it was reported by that the flow pattern transition to annular flow was observed at lower gas velocity than that under normal gravity. For the annular flow with lower gas velocity, the liquid film will be thicker. If such annular flow is obtained in boiling flows under microgravity, the boiling mode will be nucleate boiling, and vapor bubbles generated on the heat transfer surface will be contained in the liquid film.

1 Department of Mechanical Engineering, Kobe University, 1-1 Rokkodai, Nada, Kobe 657-8501, Japan
2 Department of Aeronautics and Astronautics, Kyushu University, 744 Motooka, Nishi, Fukuoka 819-0395, Japan
3 Department of Mechanical Engineering, University of Hyogo, 2167 Shosha, Himeji, Hyogo 671-2280, Japan
4 Dept. of Mech. Engineering, Tokyo University of Science, Yamaguchi, 1-1-1 Daigakudori, Sanyo-Onoda, Yamaguchi 756-0884, Japan
5 Division of Aerospace Engineering, Muroran Institute of Technology, 27-1 Mizumoto-cho, Muroran, Hokkaido 050-8585, Japan
6 IHI Aerospace, Co. Ltd., 900 Fujiki, Tomioka, Gunma 370-2398 Japan
7 Japan Aerospace Exploration Agency, 2-1-1 Sengen, Tsukuba, Ibaraki, 305-8505, Japan
8 Nara Institute of Science and Technology, 8916-5 Takayama, Ikoma, Nara 630-0192, Japan
9 Japan Space Forum, 3-2-1, Kandasurugadai, Chiyoda, Tokyo 101-0062, Japan
(E-mail: asano@mech.kobe-u.ac.jp)

Such flow condition may accelerate the liquid film or lead to an increase in the entrainment of liquid into the gas core flow. Therefore, the flow observation and measurement of the gas-liquid interface are quite important to understand the boiling and two-phase flow characteristics.

Experiments at Japanese Experimental Module "Kibo" in International Space Station (ISS) are planned to clarify boiling flow characteristics under microgravity, and are scheduled in 2016. The system design of the experimental apparatus including the kind of the working fluid had been decided, and the flight model (FM) had been constructed, and finished the performance tests. The detailed information on the purpose of the experiments and the system design concept will be described in the other papers in this issue.

Here, the two-phase flow visualization and measurement sections installed at the immediate downstream of heating test sections are introduced. The detailed specifications and the measurement items are shown with the data acquired in the function test of the engineering model (EM). The obtained results in the TPF experiments will be compared with those for vertical upward flows in the ground test facility using almost the same test sections and the working fluid. An observation section is also placed just at the downstream of each heating section. In order to evaluate the effect of boiling behaviors on the flow characteristics in the observation section, the development of the two-phase flow structure from the exit of the heating section was evaluated for vertically upward two-phase flows under normal gravity. Hazuku, et al.[7),8)] investigated the characteristics of developing vertical upward bubbly flow under normal and microgravity. The reported that the developed flow was obtained at L(length)/D(diameter) = 40 from the mixing section independent from the gravity conditions. They also investigated the developing structure of the liquid film in vertical upward annular flows. They reported that the maximum and minimum film thickness and passing frequency of disturbance waves decreased with flow development, and the developed flow could not be obtained at L/D = 250. Gregorc and Zun[9)] investigated the effect of the method of gas-liquid mixture on the position for the flow pattern transition from bubbly to slug flow in a small diameter tube. However, these previous studies were conducted for air-water two-phase flows.

In this study, to clarify the flow development characteristics of one-component two-phase flows, flow behaviors and cross-sectional average void fractions were measured at four locations at the downstream of the heating section.

2. Specifications of Experimental Loop and Observation Section for TPF Experiment

2.1 Experimental Loop

A schematic diagram of the experimental loop is shown in **Fig. 1**. The loop is a pump driven two-phase flow loop, in which

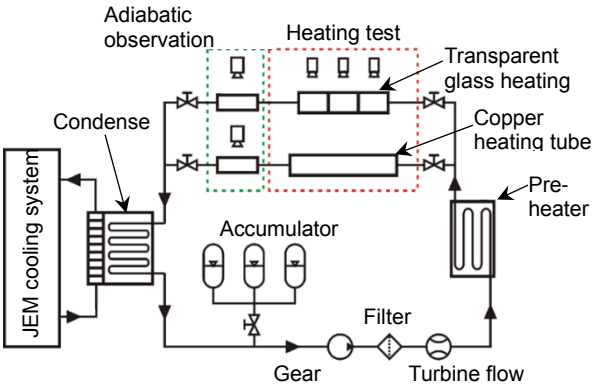

Fig. 1 Schematic diagram of the two-phase flow loop for the boiling and two-phase flow experiment on board ISS.

the fluid pressure is maintained by accumulators. Since the back pressure of the accumulator will be connected to the cabin environment, the system pressure will be around the atmospheric pressure. Perfluorohexane was selected as the working fluid. Perfluorohexane is the main component of the fluorocarbon FC-72. The saturation temperature at the atmospheric pressure is 56.9 °C. The main physical properties of perfluorohexane are shown in **Table 1** in comparison with water at the atmospheric pressure. The vapor density is about 22 times larger, and the surface tension is about one 7th smaller than water. The experimental loop has two heating sections in parallel; a copper heating tube and transparent glass heating tube. Boiling heat transfer coefficient and critical heat flux will be measured in these heating sections, and the boiling flow behaviors can be visualized in the glass tube. In order to clarify the boiling two-phase flow behaviors, observation sections are connected directly just at the downstream of each heating section. Two-phase flows from the observation section is condensed in a condenser on a cold plate by a heat exchange with a cooling water. Then, subcooled liquid returns to the mechanical pump.

2.2 Observation Section

In order to clarify the difference in flow behaviors between normal and microgravity, it is required to observe and measure gas-liquid interface structures in more detail. Especially, 3D structure should be important, because the phase distribution of vapor-liquid two-phase flows may not be axially symmetric

Table 1 Main physical properties of perfluorohexane comparing with water at the atmospheric pressure.

		perfluorohexane	water
Saturation temperature		56.9 °C.	100 °C.
Density	liquid	1621 kg/m^3	958.4 kg/m^3
	vapor	13.49 kg/m^3	0.5982 kg/m^3
Viscosity	liquid	413.3 μPa・s	281.6 μPa・s
	vapor	11.87 μPa・s	12.23 μPa・s
Surface tension		8.44 mN/m	58.9 mN/m

under microgravity. For this purpose, an observation section is introduced just at the downstream of each heating section.

The observation section was made of transparent polycarbonate resin. To make the effect of refraction at the outside wall smaller, the exterior has a rectangular shape. A circular channel with a diameter of 4 mm was drilled at the center of the rectangular column. The inner wall was carefully polished for transparency. The appearance of the observation section is shown in **Fig. 2**. The observation section is directly connected to the outlet flange of the heating section. For three-dimensional observation, a method of stereoscopic photography by which two images from two orthogonal directions can be photographed by one camera is applied. The arrangement of the optical equipment is shown in **Fig. 3**. The optical system consists of one compact high frame-rate camera whose maximum frame-rate is 1000 fps and acquirable number of frames is around 1000, four metallic mirrors, and two flicker-free LED panels for the back-lighting. Examples of the photographed images are shown in **Figs. 4 (a)** and **(b)**. These images were taken with the frame-rate of 1000 fps and the exposure time of 100 μs. The size of image pixel was about 28 μm. The three-dimensional structure of vapor-liquid interface could be visualized well. In **Fig. 4 (a)**, the bubble positions and their shapes were clearly visualized. In **Fig. 4 (b)**, the liquid film structure, especially the difference in the film thickness along the flow directions, were clearly visualized.

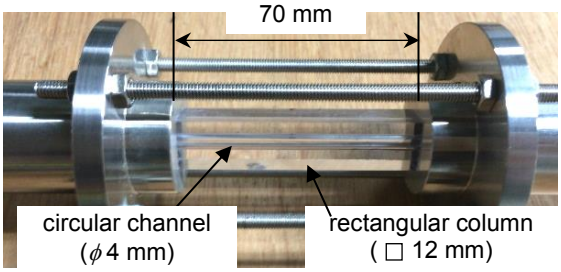

Fig. 2 Appearance of the observation section.

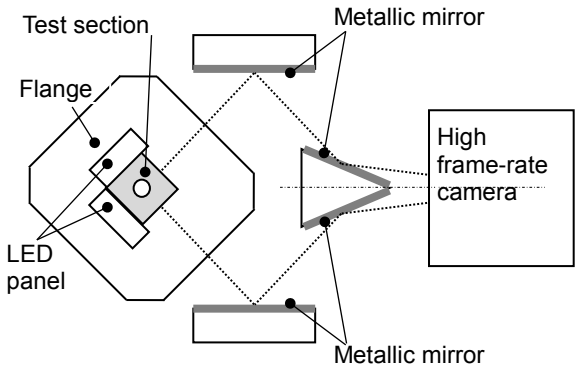

Fig. 3 Arrangement of the optical system for stereoscopic photography.

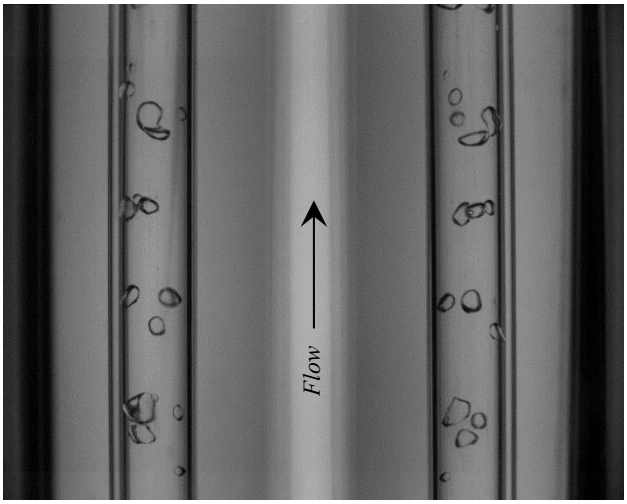

(a) Mass flux : 300 kg/(m^{2}s)

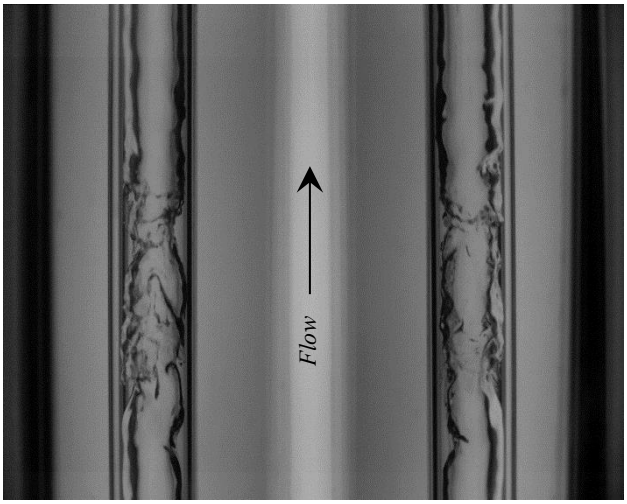

(b) Mass flux : 200 kg/(m^{2}s)

Fig. 4 Examples of the photographed images.

3. Evaluation of the Measurement Accuracy of Liquid Film Thickness

From the visualized images photographed by the high frame-rate camera, the position of gas-liquid interface can be specified considering the difference in the refraction index of the material. Bubble velocity in intermittent flows, liquid film thickness and wave velocity in annular flows, and void fraction can be measured. To evaluate the accuracy in the measurement of liquid film thickness, two methods were adopted for the calibration. The first is a static method using a stainless steel rod with various diameters from 2.0 to 3.8 mm. The rod was inserted in the tested tube filled with the liquid FC-72 to form simulated liquid films as shown in **Fig. 5**. The measured values of the thickness from the image were compared with the given thickness calculated from the difference between the inner diameter and the rod diameter. The compared results are shown in **Fig. 6**. It was seen that the actual size could be measured from the image within the error of ± 25 μm. The value was

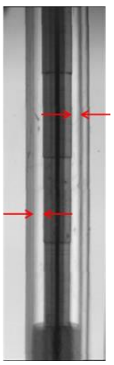

Fig. 5 Image of channel with calibration rod.

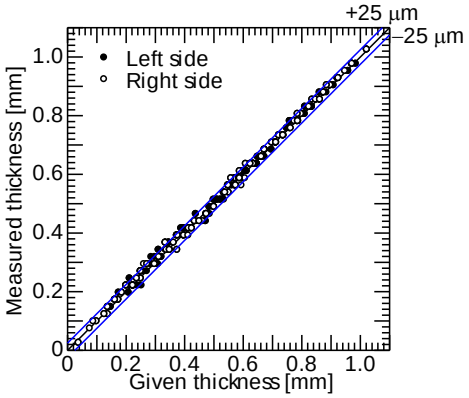

Fig. 6 Comparison of liquid thickness between measured result from image and given values using calibration rod.

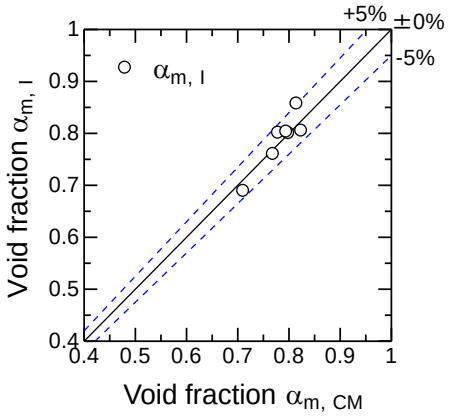

Fig. 7 Comparison of average void fractions between the measured results from the observed images, $\alpha_{m,\,I}$, and the results by a quick closing valve method, $\alpha_{m,\,CM}$.

Table 2 Comparison in refraction index.

Material	Refraction index (at 25 °C)
perfluorohexane (liquid)	1.00
perfluorohexane (vapor)	1.23
Water	1.33
Air	1.00
Acrylic resin	1.48 to 1.50
Polycarbonate resin	1.59

equivalent to the pixel size.

In the calibration by the static method, the refraction at the inside wall could be evaluated. However, the further evaluation on the effect of the refraction at the gas-liquid interface should be required. So, the measured results of time-average void fraction from the continuous images of two-phase annular flows were compared with the measured values by a quick closing valve method. Vertically downward annular flows are selected as the object, because it is difficult to detect disturbance waves by the frame-rate. For the quick closing valve method, two pneumatic normally opened ball valves were placed.at the up- and downstream of the observed section. To avoid a pressure rise caused by closing the valves, a bypass line with a pneumatic normally closed ball valve was set. The distance between two valves were 300 mm, and the observed section was placed at the center of the measurement section. The compared results are shown in **Fig. 7**. It was confirmed that the void fraction could be measured from the image within ± 5 % accuracy.

4. Development of Two-Phase Flow from the Exit of the Heating Section

In the flight model for the TPF experiment, the observation section is directly connected to the heating section. The distances from the exit of each heating section to the center of the observed section are 86 mm (L/D = 21.5) for the copper heating section and 132 mm (L/D = 32) for the glass heating section, respectively. Since the ground model to take comparable data has the same configuration for vertically upward flows, the gas-liquid interfacial structure at the measure point, especially the difference from that for the developed flow, should be clarified. Therefore, flow observation was performed and cross-sectional average void fraction was measured at four locations at the downstream of the heating section.

4.1 Experimental Loop

A schematic diagram of the experimental loop is shown in **Fig. 8**. FC-72 with almost the same thermophysical properties as perfluorohexane was used as the working fluid. The physical properties of FC-72 was obtained by the approximate expressions based on the product data. The observation sections were directly connected to the downstream of the heating tube with the inner diameter of 4 mm. A thin wall stainless steel tube was used as the heating section as shown in **Fig. 9.** The heating section was heated by Joule heating with direct current. The length of the heating section was set to the same value as the copper heating section used in the flight model. Wall temperatures of the heating tube were measured by welded thermocouples for the heat loss estimation. In the preliminary experiment for liquid single-phase flows, heat loss from the heating section was measured, and correlated to the wall temperature.

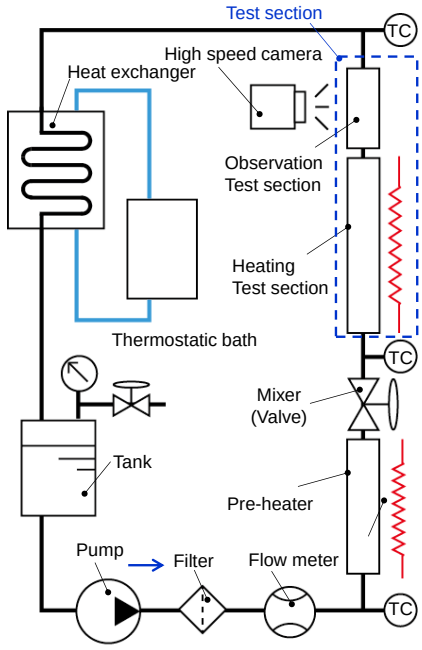

Fig. 8 Schematic diagram of experimental loop to evaluate the development of two-phase flow from the exit of the heating section.

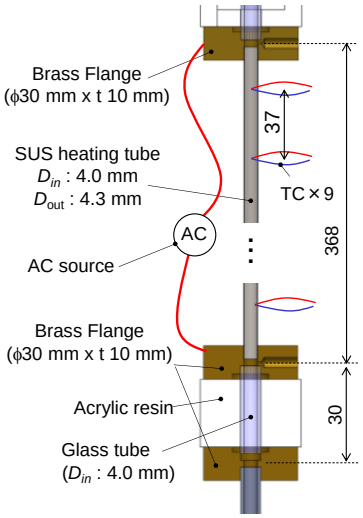

Fig. 9 Detail configuration of the heating section.

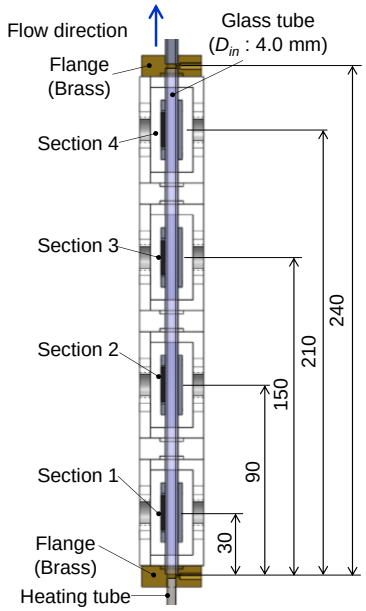

Fig. 10 Detail configuration of the observation sections.

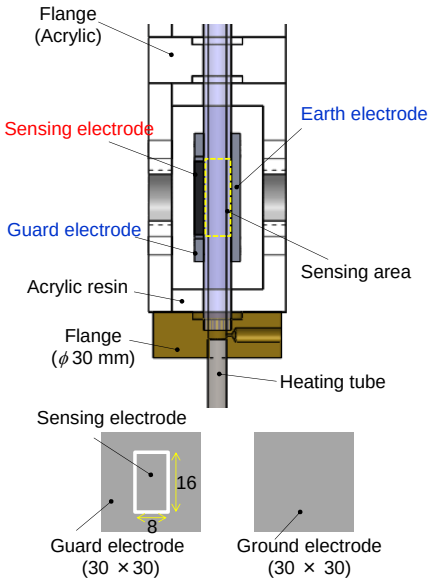

Fig. 11 Detail configuration of the capacitance sensor.

The configuration of the observation sections is shown in **Figs. 10** to **11**. Parallel electrodes type capacitance sensors were applied to measure the cross-sectional average void fraction. The length of the sensing area was 16 mm (L/D = 4) in the flow direction. Volumetric average void fractions can be measured from the capacitance, C, by the following equation.

$$\alpha_{capa} = (C_L - C) / (C_L - C_G) \quad (1)$$

where, C_G and C_L are the capacitance of vapor and liquid single-phase, respectively. The calibration of the capacitance sensor was performed by two methods. One is a static calibration by inserting a Teflon-rod instead of the liquid. The other is comparison with the measured results by a quick closing valve method. In these calibrations, the measurement accuracy of capacitance sensor was confirmed within 5 %. The detail of the calibration test had been reported by Gomyo et al.[10].

Four sensors were installed at 30 mm (L/D = 7.5), 90 mm (L/D = 22.5), 150 mm (L/D = 37.5), and 210 mm (L/D = 52.5) from the exit of the heating section. Flow behaviors could be simultaneously observed in the direction parallel to the face of the electrode, and recorded by using two high frame-rate cameras in synchronization. One was used for the section 1 and 2, and the other was used for the section 3 and 4. On the other hand, void fraction at each section was measured by switching to a high sensitivity faradmeter. The resolution of the faradmeter is 10^{-4} pF. The variation of the inlet quality in the measurements

for the 4 sections was less than ± 3 %.

Experimental conditions of mass flux and vapor quality were those for the TPF experiments at the atmospheric pressure. The inlet subcooling of the heating section was set in the range of 7 to 10 K.

4.2 Experimental Results and Discussion

Flow pattern Flow patterns observed in this experiment were classified into five regimes, i.e. slug, churn, semi-annular, and annular flow. The churn flow was defined as the flow with intermittent liquid reverse flows.

Flow pattern maps based on the observation results at each section are shown in **Fig. 12 (a)** to **(d)**, respectively. Horizontal and vertical axis show volumetric flux of gas and liquid phase, respectively. The volumetric fluxes of gas and liquid phase are defined by the following equations.

$$j_G = \frac{G \cdot x}{\rho_G}, \quad j_L = \frac{G(1-x)}{\rho_L} \qquad (2)$$

where G is mass flux, x is quality, ρ is density, and the subscripts G and L show gas and liquid phase, respectively. Bold lines show the flow pattern transition boundaries for vertical upward flows proposed by Mishima and Ishii [11].

At the section 4 (at 190 mm downstream the exit) of the heating section, the flow pattern transitions were agreed pretty well with the Mishima and Ishii's transition boundary. On the other hand, at the section 1 nearest to the exit of the heating section, the region of bubble flow and churn flow seemed to be wider. Bubble flow was observed in the flow with higher vapor volumetric flux, and churn flow was observed at lower vapor flowrate. In the condition, gas-liquid interfacial structure might change along the flow direction. In the range from section 2 to 4, the change in the flow pattern along the flow direction was a little.

Observed images in synchronization are shown in **Fig. 13 (a)** and **(b)** for the flow with quality at the heating tube exit of 0.05 and 0.36, respectively. The mass flux was 100 kg/(m^{2}s). The flow patterns for **Fig. 13 (a)** and **(b)** were slug flow and annular flow at the section 4. For the flow in **Fig. 13 (a)**, small bubbles were observed in liquid slugs at the section 1. Then, gas-liquid interface became smoother and bubble size became larger with

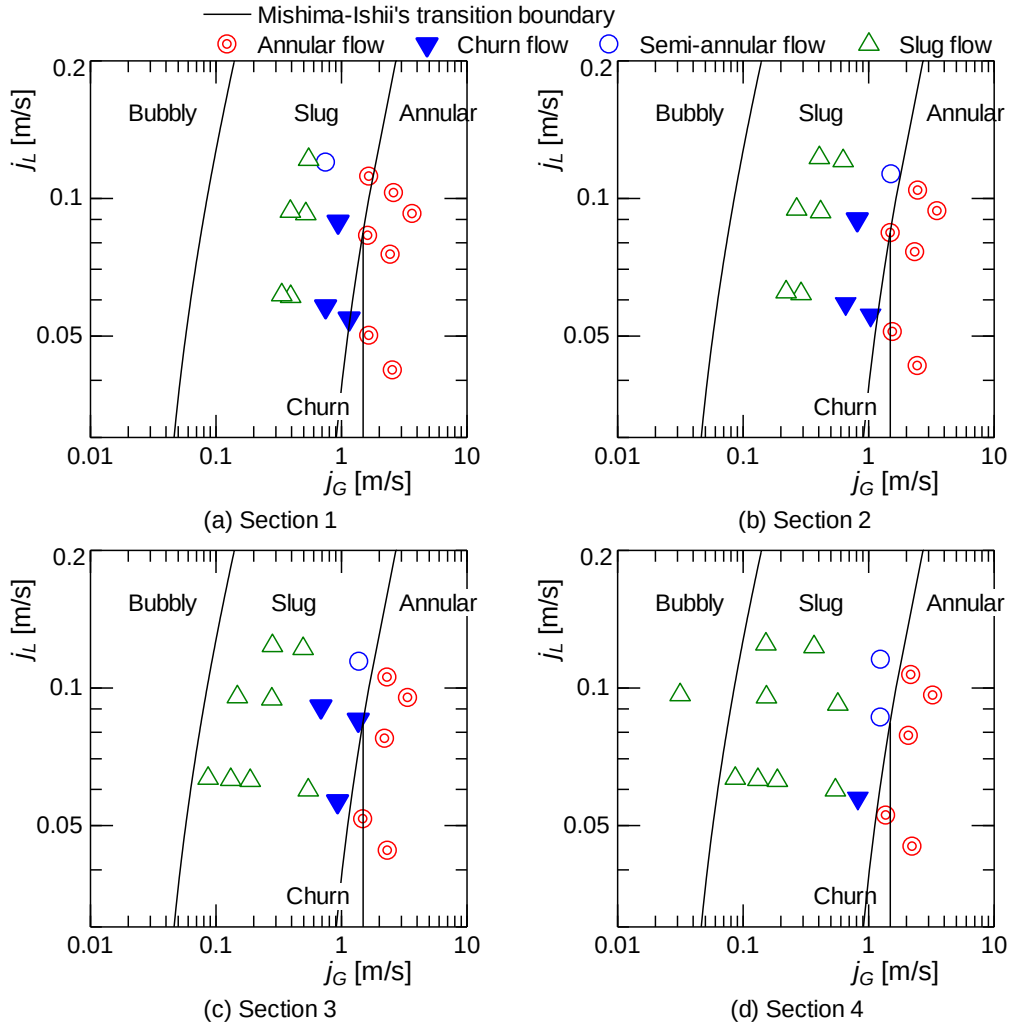

Fig. 12 Flow pattern map at each measure section.

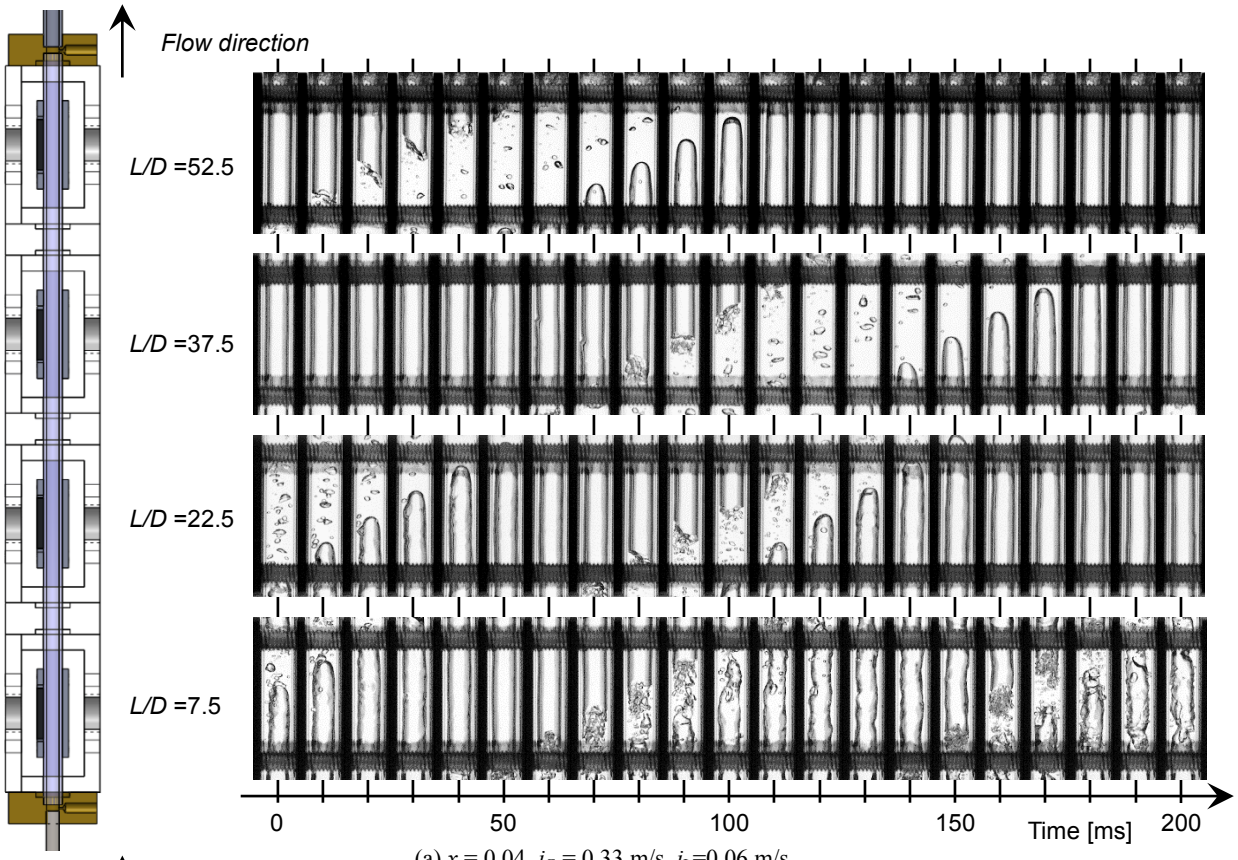

(a) $x = 0.04$, $j_G = 0.33$ m/s, j_L=0.06 m/s

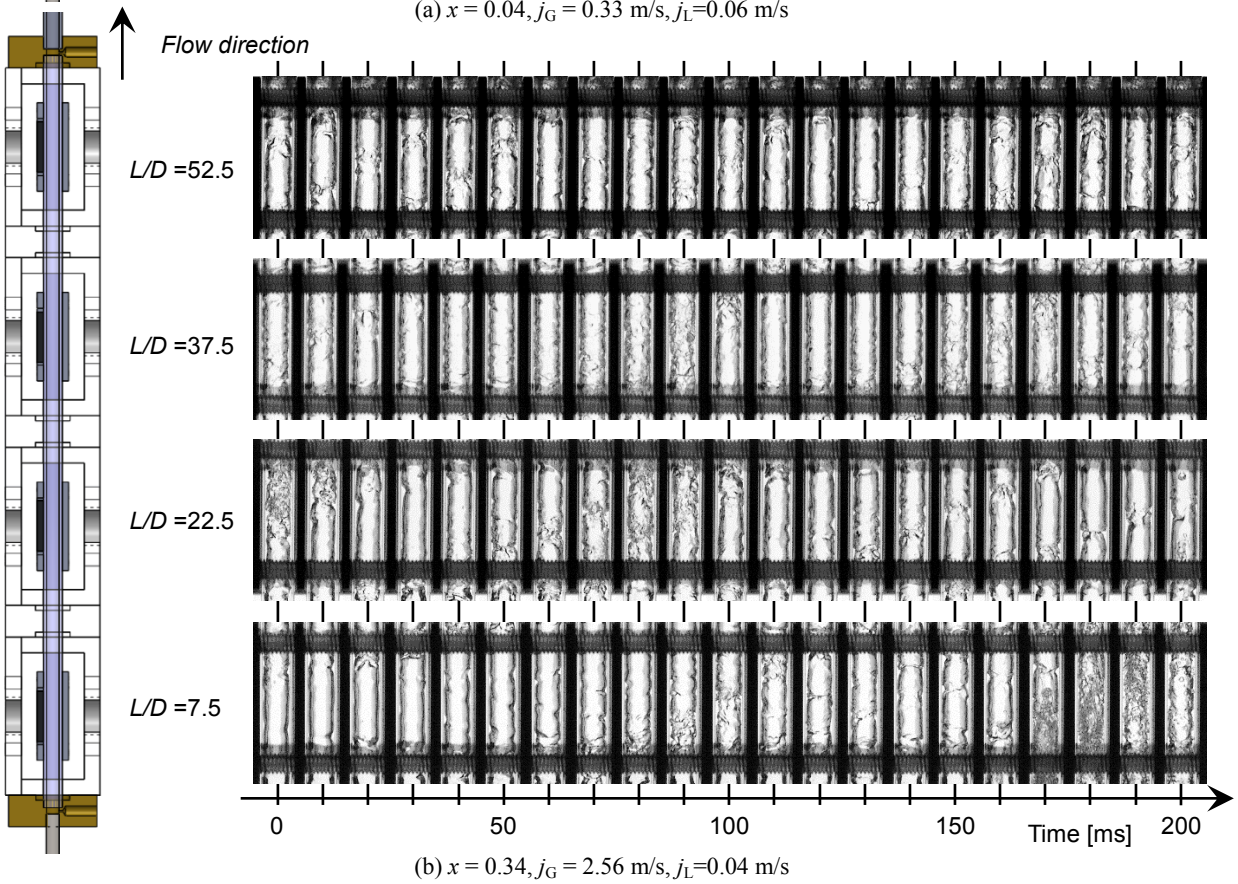

(b) $x = 0.34$, $j_G = 2.56$ m/s, j_L=0.04 m/s

Fig. 13 Change in flow behaviors from the exit of the heating section.

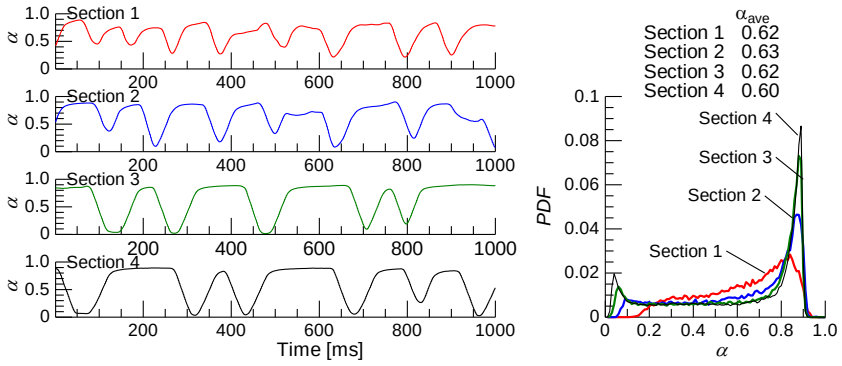

(a) $x = 0.04$, $j_G = 0.33$ m/s, j_L=0.06 m/s

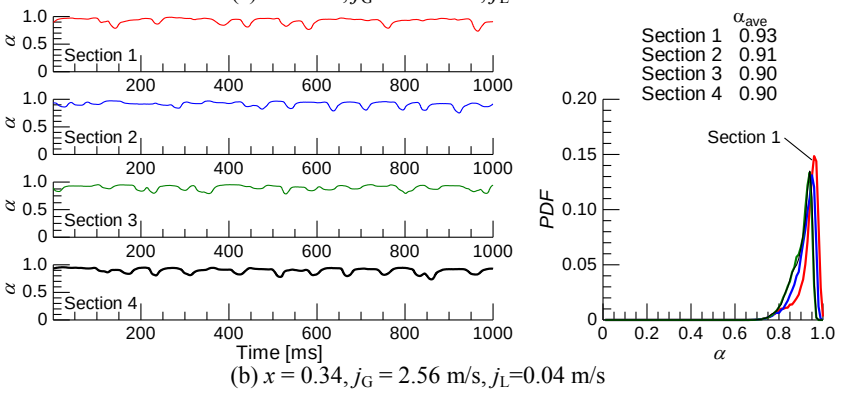

(b) $x = 0.34$, $j_G = 2.56$ m/s, j_L=0.04 m/s

Fig. 14 Void fraction fluctuation and its PDF at each measure point.

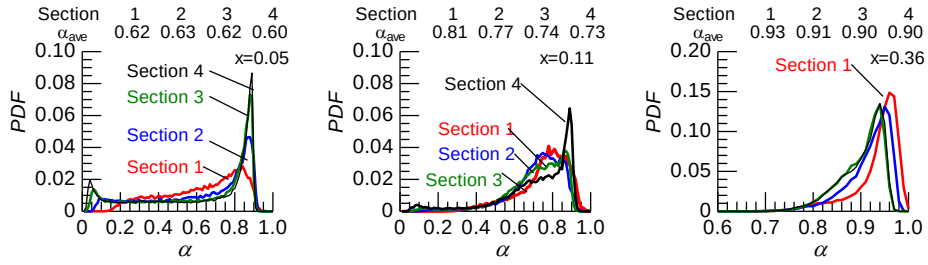

(a) $G = 100$ kg/(m^{2}s).

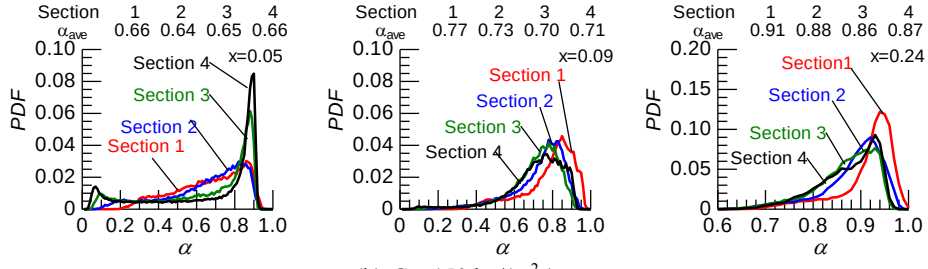

(b) $G = 150$ kg/(m^{2}s).

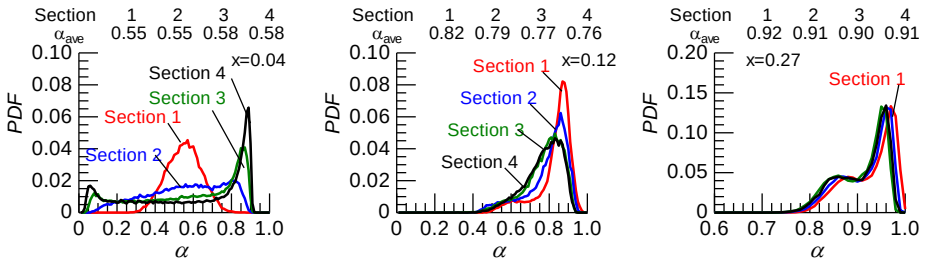

(c) $G = 200$ kg/(m^{2}s).

Fig. 15 Effect of mass flux and quality on PDF of void fraction fluctuation.

flowing downstream. For the higher quality flow in **Fig.13 (b)**, the difference in the interfacial structure was little.

Void fraction Void fraction fluctuations in the same flow conditions are shown in **Fig. 14** with the related probability density function. Each PDF was obtained from the recorded data during 60 seconds with the sampling frequency of 1 kHz. For the slug flow shown in **Fig. 14 (a)**, it could be seen in the PDFs that at the section 1, the distribution was broad with a peak around 0.8, because many small bubbles in nucleate boiling were continuously flowing out. However, in the downstream from the section 2, another peak at low void fraction less than 0.1 was formed. The two peaks mean the formation of vapor slug as a result of bubble coalescence. The time average values were almost the same.

On the other hand, for the annular flow shown in **Fig. 14 (b)**, liquid film at the section 1 was a little smoother and thinner. At the section 2 (L/D = 22.5), the liquid film became a little thicker and had almost the same structure with the developed one.

Figure 15 shows the comparison in PDFs among the measure sections for various flow conditions of mass flux and vapor quality. For the lowest quality condition of each mass flux, the same tendency with the slug flow in **Fig. 14 (a)** was observed, and the difference became larger with increasing the mass flux. For the highest quality condition of each mass flux, the flow patterns were annular flows, and the effect of the location became smaller with increasing the mass flux. In the PDF of the annular flow with the mass flux of 200 kg/(m^2s) and quality of 0.27, a second peak around 0.85 was observed. The peak means the existence of disturbance waves.

4. Conclusions

An observation section has been developed for the detail observation of gas-liquid interfacial structure in boiling and two-phase flow experiments onboard International Space Station. A stereoscopic photography method was applied for 3D measurement using one high frame-rate camera. It was confirmed that the liquid film thickness could be measured from the images within ± 5 % accuracy. Moreover, the development of the flow structure from the exit of the heating section was evaluated from the results of the flow observation and the cross-sectional average void fraction measurement at the four locations places at the downstream of the heating section. As a result, under the conditions where slug flow was observed in the developed region, the fluctuation band of void fraction was small just downstream the exit of the heating section due to many small bubbles in liquid slugs. Under the conditions where annular flow was observed in the developed region, annular flow had been already formed at the exit of the heating section, and then liquid film thickness became thicker.

References

1) M. Narcy and C. Colin: Interfacial Phenomena and Heat Transfer, **3** (2015) 1.
2) M. Narcy, E. De Malmazet and C. Colin: Int. J. Multiphase Flow, **60** (2014) 50.
3) M. Saito, N. Yamaoka, K. Miyazaki, M. Kinoshita and Y. Abe: Nuclear Engineering and Design, **146** (1994)451.
4) H. Ohta: Nuclear Engineering and Design, **175** (1997)167.
5) H. Ohta: Advances in Heat Transfer, **37** (2003) 1.
6) H. Ohta and S. Baba: Experimental Heat Transfer, **26** (2013) 266.
7) T. Hazuku, T. Takamasa and T. Hibiki: Int. J. Multiphase Flow, **38** (2012) 53.
8) T. Hazuku, T. Takamasa and Y. Matsumoto: Int. J. of Multiphase Flow, **34** (2008) 111.
9) J. Gregorc and I. Zun: Chem. Eng. Sci., **102** (2013) 106.
10) T. Gomyo, H. Asano, H. Ohta, Y. Shinmoto, O. Kawanami, T. Kurimoto, M. Komasaki and S. Matsumoto: Japanese J. of Multiphase Flow, **27** (2014) 437 (in Japanese).
11) K. Mishima and M. Ishii: Int. J. Heat and Mass Transfer, **27** (1984) 723.

Int. J. Microgravity Sci. Appl., **33** (1) (2016) 330104
DOI: 10.15011/ijmsa.33.330104

